Optical humidity sensing and ultrasound effect for mesoporous silicon one-dimensional photonic crystals

I. G. Kolobov,[1] William B. Euler,[1] and I. A. Levitsky[1,2,*]

[1]Department of Chemistry, University of Rhode Island, Kingston, Rhode Island 02881, USA

[2]Emitech, Inc., Fall River, Massachusetts, 02720, USA

*Corresponding author: ilevitsky@chm.uri.edu

Received 16 October 2009; revised 2 December 2009; accepted 4 December 2009; posted 4 December 2009 (Doc. ID 118570); published 24 December 2009

Mesoporous silicon (PSi) microcavities (MC) based on one-dimensional photonic crystals have been studied as optical sensors for relative humidity (RH). Oxidized PSi modified the structure of the MC such that the spectral position of the MC resonance peak depended on the humidity. A spectral shift of the MC resonance peak of up to 6 nm to longer wavelengths was observed as the RH increased from 20% to 85%. Ultrasound affects the MC peak spectral position in the reverse direction as a result of water removal from mesoporous structure. This effect can be used for the stabilization of the peak spectral position for an optical interconnect and fast recovery of the optical gas sensors. © 2009 Optical Society of America

OCIS codes: 280.4788, 050.5298.

1. Introduction

Porous silicon (PSi) based chemical and biological optical sensors have been intensively studied for the past decade [1–10] because of the high surface area of PSi and the variety of optical transduction mechanisms upon exposure to different analytes. Optical sensors based on PSi one-dimensional photonic crystals with microcavity [3–10] demonstrated better sensitivity than PSi monolayers or Bragg mirrors due to the existence of a sharp resonance peak in the reflectance spectrum whose spectral position depends on the change of the microcavity (MC) refractive index. In the case of the vapor sensing, two major mechanisms responsible for the refractive index change can be considered: capillary condensation (relatively high vapor pressure) and physisorption on the inner walls of PSi (low vapor pressure). In addition, for MCs infiltrated with sensory polymers [10], chemisorption contributes to the refractive index change.

Among the variety of vapors tested in PSi MC optical sensors [3–10], just a few reports are related to humidity sensing [4,11], probably because the MC resonance peak in these studies was almost unresponsive to the humidity change (e.g., 0.4 nm redshift from dry to 50% relative humidity [11]). Mulloni *et al.* [4] reported no change of the MC peak spectral position even for immersion of MC in water. It is worth mentioning that MCs in these reports were not oxidized at high temperatures under oxygen or at normal conditions with ozone exposure. As a result, the porous surface was terminated mostly by Si-H groups making it hydrophobic, which prevents water vapor condensation.

As we demonstrate in this study, the resonance peak of highly oxidized MC can be sensitive to water vapor (up to 6 nm shift from dry to 85% relative humidity) providing a simple design for an optical humidity sensor. To our knowledge, to date only capacitance/conductive humidity sensors based on porous Si have been reported in the literature [12–14]. Optical sensors have advantages over electrical sensors because of their fast response and the absence of electrodes (or electrode/PSi interface) that could be

0003-6935/10/010137-05$15.00/0

affected by sensing analytes. Another aspect reported in this study is the influence of the ultrasound (~5 MHz) on the MC optical properties leading to water evaporation followed by the shift of the MC resonance peak to shorter wavelengths: essentially "MC drying." This new effect can be employed for resonance peak stabilization at varied environmental conditions. Moreover, ultrasound is capable of efficiently removing not only condensed water but also organic molecules sorbed by the PSi structure.

2. Experiment

The PSi MCs fabrication is described elsewhere [10]. Briefly, they were prepared by anodic etching of *p*-type (100)-oriented Si wafers (resistivity ~0.01 Ω cm) in 15% solution of HF with ethanol. The microcavity structure consists of a Fabry–Perot resonator between two distributed Bragg reflectors (DBRs) that are fabricated from alternating layers of high and low porosity. Anodization was performed under a periodically changing current applied between a silicon wafer and a platinum electrode. In fabricated samples, the first DBR consists of 5 periods, while the second has 20 periods; each period contains two layers, high and low porosity. For most samples, the low and high porosity layers were fabricated at a current density of 6 mA/cm^2 and 25 mA/cm^2, respectively. MCs were oxidized at 900 °C under oxygen flow for 20 min. The reflectance spectra were measured with an Ocean Optics spectrometer coupled with an optical fiber positioned normal to the sample surface. An ultrasound transducer (NDT Olympus A126S-RM, resonance frequency −5 MHz, FWHM −4 MHz, maximum power −125 mW) working under AC sinusoidal voltage from a functional generator was coupled with the back side of MC through the silicon grease. The silicon grease (Olympus Couplant C silicone oil) was deposited on the back side of the Si wafer as a thin layer (~3 mm), followed by firmly pressing to the transducer surface. The samples were placed in a custom designed test chamber (30 ml) equipped with a flow controller to regulate the humidity or vacuum level.

3. Results and Discussion

Figure 1(a) shows the reflectance spectra of as-prepared mesoporous MC (pore size in the range of 5–10 nm) and after oxidation at 900 °C. The scanning electron microscope image of the PSi structure (monolayer etched at 30 mA/cm^2) is shown in Fig. 1(b). The sizable blueshift of the resonance peak is observed, which is indicative of Si oxidation. We found that oxidized MC is sensitive to the relative humidity (RH) level: the MC resonance peak demonstrates a redshift of up to 6 nm [Fig. 2(a)] upon RH increase from 20% to 85%. In contrast, nonoxidized MC is almost unresponsive to the RH change (redshift less than 0.5 nm), which is consistent with previously reported results [4,11]. The dependence of the MC shift on RH is a nonlinear function. Therefore, approximately the sensitivity to RH was extracted from the slope of the straight lines [Fig. 2(a)] for two ranges 20–60% and 60–85%, which corresponds to 0.0725 nm/% RH and 0.143 nm/% RH, respectively.

Ultrasound also affects the MC resonance peak resulting in a blueshift at sufficient RH level [Fig. 2(b)], similar to air pumping from MC [Fig. 2(c)]. At low humidity (at 20–30% and less) no noticeable spectral shift under ultrasound or vacuum was observed. These results can be interpreted in terms of water removal from the mesoporous structure of PSi MC, although the heating of porous Si upon ultrasound could be an alternative explanation. As reported by Weiss *et al.* [15], the increase of temperature resulted in a blueshift of the resonance peak for an oxidized microcavity. However, the heating effect can be ruled out since the temperature change does not exceed 2 °C at the maximum ultrasound power (temperature was measured with an accuracy of 0.2 °C by a miniature thermistor attached to the MC surface). Such a small temperature elevation cannot be the cause of a blueshift of up to 6 nm as demonstrated by the temperature dependence of the spectral position of the MC peak presented in the inset of Fig. 2(b).

To elucidate the situation with water condensation and its removal by ultrasound, five PSi monolayers of different porosity were prepared (Table 1). As shown in Table 1, there is a correlation between the spectral shift of the Fabry–Perot fringes and porosity of the monolayers. The highest spectral shift (4 nm for

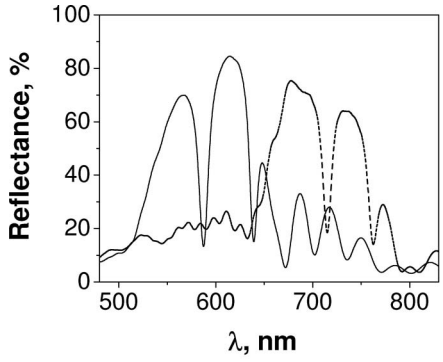

(a)

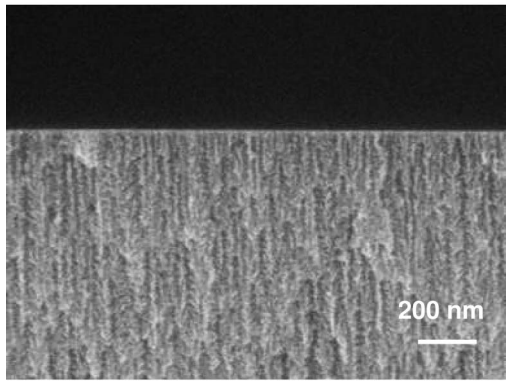

(b)

Fig. 1. (a) Reflectance spectra of the fresh prepared PSi MC (dashed line) and after annealing (solid line). (b) SEM image of the cross section of porous Si etched at 30 mA/cm^2.

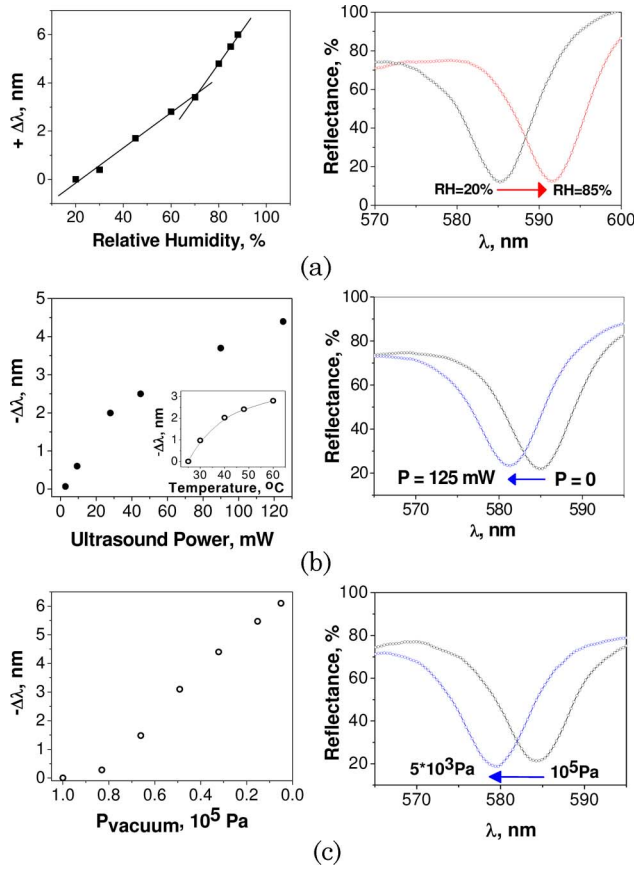

Fig. 2. (Color online) (a) Dependence of the spectral shift of MC peak on RH% at 22 °C and MC spectral position for RH = 20% (black) and RH = 85% (red). (b) Dependence of the spectral shift of MC peak on ultrasound power P at RH = 85% and MC spectral position for $P = 0$ mW (black) and $P \sim 125$ mW (blue). Inset shows the MC peak spectral shift on temperature. (c) Dependence of the spectral shift of MC peak on air pressure, at RH = 85% and MC spectral position for pressure of 10^5 Pa (black) and 5×10^3 Pa (blue).

vacuum and 2.5–3 nm for ultrasound) is observed for monolayer with low porosity (43%), and practically no shift was detected for high porosities (more than 75%). These results are in a good agreement with the capillary condensation model, where the average pore radius is responsible for critical vapor condensation inside the mesopores. This process can be described by the Kelvin formula [16] for relative vapor pressure P at which condensation occurs for pores of radius r:

$$\frac{P}{P_S} = \exp\left(-\frac{\gamma V_L}{RTr}\right), \tag{1}$$

where γ is the surface tension of the liquid, V_L is the molar volume of the liquid, R is the gas constant, T is temperature, and P_s is the saturation vapor pressure of the liquid. Thus, pores with small radius (low porosity) facilitate and make more effective water vapor condensation as compared with pores with large radius (high porosity).

The use of the Bruggeman approximation [17] can provide the value of the water volume fraction as a function of the porosity. However, it is difficult to calculate the volume fractions of SiO_2 and Si that are formed after annealing. Nevertheless, the water fraction can be estimated for the low porous layer (43.5% porosity, Table 1), assuming that the major contribution to the effective dielectric constant is associated with silicon, and neglecting the SiO_2 volume fraction. This is consistent with the similarity between $L_{2,3}$ X-ray emission spectra of annealed low porous Si and bulk silicon [18]. According to the Bruggeman model, an effective dielectric constant of the medium ε_{av} composed from n components can be defined from the equation

$$\sum_i^n \rho_i \left[\frac{(\varepsilon_i - \varepsilon_{av})}{(\varepsilon_i + 2\varepsilon_{av})}\right] = 0, \tag{2}$$

where ε_i and ρ_i are the dielectric constant and volume fraction of each component, respectively. For a three-component medium,

$$\rho\left[\frac{(\varepsilon_{si} - \varepsilon_{av})}{(\varepsilon_{si} + 2\varepsilon_{av})}\right] + (1 - \rho - \rho_w)\left[\frac{(\varepsilon_{\text{air}} - \varepsilon_{av})}{(\varepsilon_{\text{air}} + 2\varepsilon_{av})}\right] + \rho_w\left[\frac{(\varepsilon_w - \varepsilon_{av})}{(\varepsilon_w + 2\varepsilon_{av})}\right] = 0, \tag{3}$$

where ε_{si}, ε_{air}, and ε_w are the dielectric constant of Si, air, and water, ρ is the layer porosity, and ρ_w is the water volume fraction. Initially, Eq. (3) is solved for two components to obtain the $\varepsilon_{av}{}^0$ value without the water component, followed by solving Eq. (3) taking into account $\varepsilon_{av} = \varepsilon_{av}{}^0 + \Delta\varepsilon_{av}{}^0$, where $\Delta\varepsilon_{av}{}^0/\varepsilon_{av}{}^0 = 2\Delta\eta_{\text{eff}}/\eta_{\text{eff}}$ (Table 1). Finally, the water fraction $\varepsilon_w = 3.9\%$ was obtained for RH = 85%. Thus

Table 1. Characteristics of PSi Monolayers of Different Porosity and the Spectral Shift of Their Fabry-Perot Fringes (at 600 nm) Upon Ultrasound Power ($-\Delta\lambda_{\text{US}}$) and Pressure ($-\Delta\lambda_{\text{VAC}}$)

Samples	I mA/cm^2	Porosity,%	$-\Delta\lambda_{\text{US}}$, nm [a]	$-\Delta\lambda_{\text{VAC}}$, nm [b]	n_{eff}	$\Delta n_{\text{eff}}/n_{\text{eff}}$ [c]
1	5	43.5	2.5	4	3.4	6.9×10^{-3}
2	10	51.0	1	2	3.2	3.4×10^{-3}
3	30	61.2	~0.5	1.6	3.0	2.7×10^{-3}
4	60	75.2	-	~0.8	2.3	-
5	80	83.7	-	-	1.8	-

[a] Spectral shift was detected for ultrasound power of 125 mW (RH = 85%).
[b] Spectral shift was detected for vacuum of 5×10^3 Pa.
[c] n_{eff} was calculated according to formula $n_{\text{eff}} = 2d(\lambda\lambda_1)/(\lambda - \lambda_1)$, where $d = 2\,\mu$m($\pm$10%) for all monolayers, and $\Delta n_{\text{eff}} = n_{\text{eff}} 2d\Delta\lambda/\lambda_1$ for vacuum of 5×10^3 Pa.

the spectral shift of 6 nm at RH = 85% corresponds the water fraction of ~4% in low porous Si. These data correlate with results of study [9], where the similar shifts and corresponding values of the liquid fractions in mesoporous Si were calculated upon exposure of several organic vapors.

Note that the refractive index of bulk water (1.3) can be changed owing to quantum confinement inside the mesoporous structure. In such a nanoenvironment, water can exist in the form of clusters, and its physical and chemical properties are distinct from the bulk substance [19,20].

The dynamics of the water removal under ultrasound [Fig. 3(a)] is different from the vacuum effect [Fig. 3(b)]. This mechanism is far from fully understood. We can speculate that a cavitation effect inside the water clusters contributes to water removal from the pores. Acoustic cavitation results in growth and collapse of bubbles in liquids leading to local temperature increase up to several thousands of Kelvin [21]. Such extreme conditions should release the water from the mesoporous medium. The recovery process (complete return of the MC peak to the initial spectral position) for the ultrasound effect is characterized by a much longer time than for vacuum and can be associated with relatively slow back diffusion of the water molecules and their condensation inside the nanopores. In the case of the vacuum, the recovery time should be similar to the response time, as the fast increase of the pressure (usually takes ~1–2 s) forces the water molecules to quickly infiltrate back into the mesoporous structure. This assumption is consistent with the experimental data [Fig. 3(b)]. We did not find any dependence of the MC spectral shift on ultrasound frequency in the range from 2 MHz to 8 MHz.

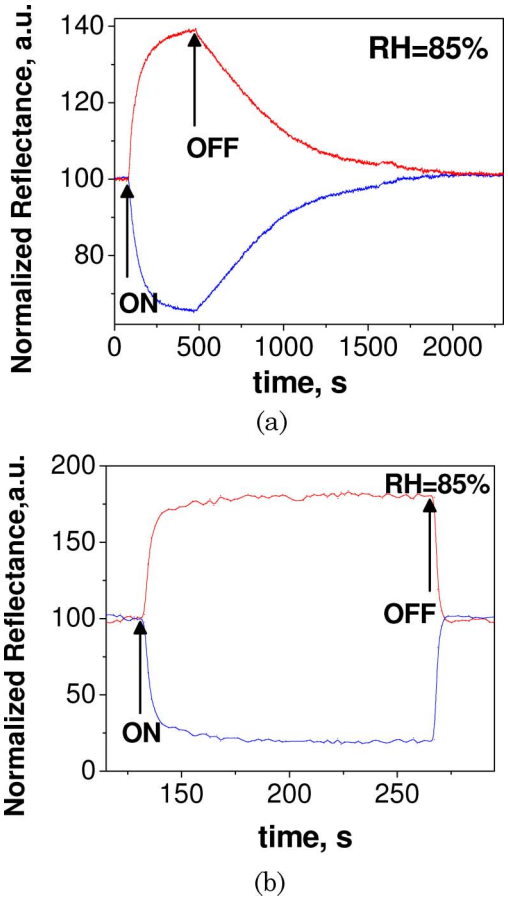

Fig. 3. (Color online) Time traces of the normalized reflectance for ON/OFF cycle of applied ultrasound power (a) and vacuum (b). Reflectance intensities were taken on the half-width of the MC peak for short wavelength (blue) and long wavelength (red) shoulders. Ultrasound power is ~125 mW and final air pressure is 5×10^3 Pa (RH = 20%).

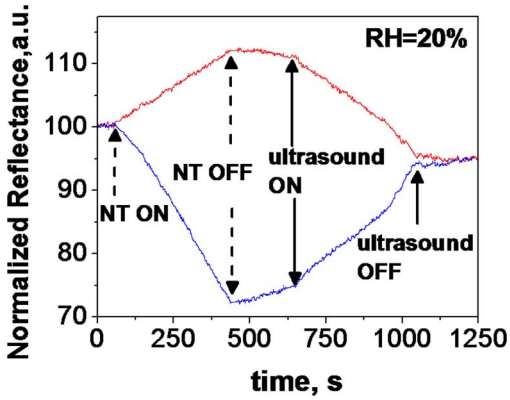

Fig. 4. (Color online) Time traces of the normalized reflectance upon exposure of saturated vapors of nitrotoluene (NT) followed by 125 mW ultrasound ON/OFF cycle. Reflectance intensities (blue and red) are the same as in Fig. 3 (RH = 20%).

Ultrasound can be applied to remove not only water but also organic compounds condensed inside the MC mesopores. Figure 4 demonstrates the dynamics of MC peak spectral position upon exposure of nitrotoluene saturated vapors followed by ultrasound application. Without ultrasound, the natural recovery takes about 30 min, while with ultrasound the recovery time does not exceed 5–6 min. Such effect can be employed for effective recovery of gas sensors based on porous Si.

4. Conclusions

In conclusion, we have demonstrated that a highly oxidized Si microcavity can be used as a simple and efficient optical humidity sensor. The transduction mechanism is the correlation between the spectral position of the MC resonance peak and RH level. Water condensed inside SiO_2 mesopores can be removed by ultrasound, resulting in a spectral shift of the MC resonance peak. This effect can be applied for fine tuning of the peak spectral position (or peak stabilization in changing environmental conditions), which can be beneficial for an optical interconnect. Moreover, ultrasound is capable of efficiently removing both condensed water and organic molecules sorbed inside mesopores that can be used for the fast recovery of PSi optical gas sensors.

The authors are grateful to Dr. A.D. Rozenberg for the helpful discussion and stimulating interest in ultrasound effect.

References

1. P. A. Snow, E. K. Squire, P. J. Russel, and L. T. Canham, "Vapor sensing using the optical properties of porous silicon Bragg mirrors," J. Appl. Phys. **86**, 1781–1784 (1999).
2. M. Ben-Chorin, A. Kux, and I. Schechter, "Adsorbate effects on photoluminescence and electrical conductivity of porous silicon," Appl. Phys. Lett. **64**, 481–483 (1994).
3. J. J. Saarinen, S. M. Weiss, P. M. Fauchet, and J. E. Sipe, "Optical sensor based on resonant porous silicon structures," Opt. Express **13**, 3754–3764 (2005).
4. V. Mulloni and L. Pavesi, "Porous silicon microcavities as optical chemical sensors," Appl. Phys. Lett. **76**, 2523 (2000).
5. S. Chan, S. R. Horner, P. M. Fauchett, and B. L. Miller, "Identification of gram negative bacteria using nanoscale silicon microcavities," J. Am. Chem. Soc. **123**, 11797–11798 (2001).
6. V. S. Y. Lin, K. Motesharei, K. P. C. Dancil, M. J. Sailor, and M. R. Chadiri, "A porous silicon-based optical interferometric biosensor," Science **278**, 840–843 (1997).
7. C. Pacholski, M. Sartor, M. J. Sailor, F. Cunin, and G. M. Miskelly, "Biosensing using porous silicon double-layer interferometers: reflective interferometric Fourier transform spectroscopy," J. Am. Chem. Soc. **127**, 11636–11645 (2005).
8. L. De Stefano, L. Moretti, I. Rendina, and A. M. Rossi, "Porous silicon microcavities for optical hydrocarbons detection," Sens. Actuators A, Phys. **104**, 179–182 (2003).
9. L. De Stefano, R. Moretti, I. Rendina, S. Tundo, and A. M. Rossi, "Smart optical sensors for chemical substances based on porous silicon technology," Appl. Opt. **43**, 167–172 (2004).
10. A. Levitsky, W. B. Euler, N. Tokranova, and A. Rose, "Fluorescent polymer-porous silicon microcavity devices for explosive detection," Appl. Phys. Lett. **90**, 041904 (2007).
11. C. Baratto, G. Faglia, G. Sberveglieri, Z. Gaburro, L. Pancheri, C. Oton, and L. Pavesi, "Multiparametric porous silicon sensors," Sensors **2**, 121–126 (2002).
12. P. Furjes, A. Kovacs, Cs. Dücso, M. Ádam, B. Muller, and U. Mescheder, "Porous silicon-based humidity sensor with interdigital electrodes and internal heaters," Sens. Actuators B **95**, 140–144 (2003).
13. Z. M. Rittersma, A. Splinter, A. Bödecker, and W. Benecke, "A novel surface-micromachined capacitive porous silicon humidity sensor," Sens. Actuators B **68**, 210–217 (2000).
14. J. J. Mares, J. Kristofic, and E. Hulicius, "Influence of humidity on transport in porous silicon," Thin Solid Films **255**, 272–275 (1995).
15. S. M. Weiss, M. Molinari, and P. M. Fauchet, "Temperature stability for silicon-based photonic band-gap structures," Appl. Phys. Lett. **83**, 1980–1983 (2003).
16. S. J. Gregg and K. S. Sing, *Adsorption, Surface Area and Porosity*, 2nd ed. (Academic, 1982), p. 112.
17. C. F. Bohren and D. R. Huffman, *The Absorption and Scattering of Light By Small Particles* (Wiley, 1983), p. 217.
18. J. McLeod, E. Z. Kurmaev, P. V. Sushko, A. Moewes, and A. I. Levitsky, "X-ray spectroscopy detection of nitroexplosive vapors adsorbed in mesoporous silicon," Phys. Rev. Lett. (to be published).
19. Y.-C. Liu, Q. Wang, and L.-H. Lu, "Water confined in nanopores: its molecular distribution and diffusion at lower density," Chem. Phys. Lett. **381**, 210–215 (2003).
20. V. Garbuio, C. Andreani, S. Imberti, A. Pietropaolo, G. F. Reiter, R. Senesi, and M. A. Ricci, "Proton quantum coherence observed in water confined in silica nanopores," J. Chem. Phys. **127**, 154501 (2007).
21. E. B. Flint and K. S. Suslick, "The temperature of cavitation," Science **253**, 1397–1399 (1991).